

Incremental adaptation of a robot body schema based on touch events

Rodrigo Zenha¹, Pedro Vicente¹, Lorenzo Jamone^{2,1} and Alexandre Bernardino¹

Abstract—The term ‘body schema’ refers to a computational representation of a physical body; the neural representation of a human body, or the numerical representation of a robot body. In both humans and robots, such a representation is crucial to accurately control body movements. While humans learn and continuously adapt their body schema based on multimodal perception and neural plasticity, robots are typically assigned with a fixed analytical model (*e.g.*, the robot kinematics) which describes their bodies. However, there are always discrepancies between a model and the real robot, and they vary over time, thus affecting the accuracy of movement control. In this work, we equip a humanoid robot with the ability to incrementally estimate such model inaccuracies by touching known planar surfaces (*e.g.*, walls) in its vicinity through motor babbling exploration, effectively adapting its own body schema based on the contact information alone. The problem is formulated as an adaptive parameter estimation (Extended Kalman Filter) which makes use of planar constraints obtained at each contact detection. We compare different incremental update methods through an extensive set of experiments with a realistic simulation of the iCub humanoid robot, showing that the model inaccuracies can be reduced by more than 80%.

I. INTRODUCTION

Humans develop a neural representation of their body (*i.e.*, a body schema [1]) through an incremental learning process that starts in early infancy [2], and likely even prenatally [3], and goes through continuous adaptations over time, based on multimodal sensorimotor information acquired during motor experience [4]: visual, tactile, proprioceptive. This (physical) body schema is a crucial part of human self-awareness and it supports the precise control of body movements, coping with the morphological changes that occur in the body over time, *e.g.*: body growth, tool assimilation.

Clearly, endowing artificial agents with similar learning and adaptation capabilities is a major challenge for cognitive robotics and it paves the way for the next generation of robots able to act in complex environments. An accurate model of the robot structure (*i.e.*, kinematics) are required for nearly all robotic tasks, to interact with objects and even more crucially to safely interact with people [5]. A variety of factors, such as difficult-to-model transmissions, friction, worn joints and bended rigid bodies, induce changes to the robot kinematic model over time. As a consequence, robots need to perform off-line calibration procedures from time to time in order to preserve their reliability. However,

¹ Institute for Systems and Robotics, Instituto Superior Técnico, Universidade de Lisboa, Lisbon, Portugal. rodrigo.n.zenha@tecnico.ulisboa.pt , {pvicente, alex}@isr.tecnico.ulisboa.pt

² ARQ (Advanced Robotics at Queen Mary), School of Electronic Engineering and Computer Science, Queen Mary University of London, UK l.jamone@qmul.ac.uk

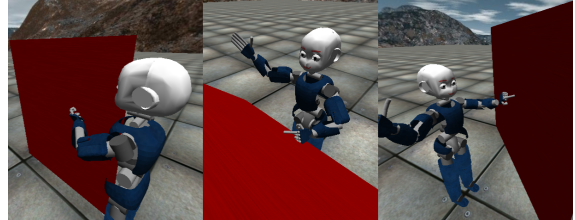


Fig. 1. Simulation of an iCub robot reaching for three different walls in its workspace.

such procedures are time-consuming, they require to stop the robot normal operations, and they need to be triggered by an explicit detection of a miscalibration issue. Online incremental procedures that can be performed by the robot during its normal operations are therefore more desirable, in any robotic application. Humanoid robots, such as the iCub [6] (shown in Fig. 1), typically rely on on-board sensors to control their movements, and therefore it would be best to perform such continuous calibration based on them without having external devices. Ideally, information from different on-board sensors should be combined to increase the robustness and reliability of the calibration (*i.e.*, an incremental self-body schema adaptation).

In this work we develop an incremental calibration strategy that is performed automatically by the robot during the execution of any arm movement that involves contacts on known planar surfaces, using the Extended Kalman Filter for adaptive parameter estimation. To do so, we make use of contact (pressure sensitive fingertips) and proprioception (joint encoders) sensors, commonly present in many humanoid robots, such as the iCub. Notably, we compare six different approaches for the update of the body schema from new data obtained after each contact with a surface, by performing an extensive set of experiments with a simulated iCub robot. Interestingly, our techniques are robot-independent, and they could be used on any robot equipped with joint angle position sensors and contact sensing capabilities at the end-effector (*e.g.*, pressure, force or acceleration sensors).

II. RELATED WORK

Robots and humans need to have an accurate model of their bodies to be able to reach and manipulate objects. To do so, robots typically rely on an analytical model which enables them to perform motion control.

A number of works have been developed in order to make use of sensory feedback, mainly visual, so as to actively estimate the robot’s hand pose and visually controlling reaching tasks [7], [8], [9], [10]. The techniques proposed

in previous works provide an efficient way of controlling motion towards a specific non-occluded object, but they do not help the robot to make use of model-based planners to control more general motions. We can find in literature methods that compensate for local errors during the robot's manipulator trajectory (*e.g.*, using visual servoing) [7], [11], however, these works do not consider sensorimotor data to actively learn an internal model representation.

Body schema learning has been widely studied (check [12] and [13] for work review on this topic). In robotics, we can formulate the adaptation of the robot body schema as a self-calibration problem, where the robot's internal model parameters are estimated (learned) online during motor experience. Some works first attempt to solve the body schema and hand pose estimation by using either a camera attached to a moving end-effector matching points in the scene from consecutive frames [14], or Laser Tracking Systems (LTS) to track a marker placed on the end-effector in order to secure a robust calibration [15]. Both cases make use of sensors that are not usual to humanoid robots.

Contact information was used in [16] to develop an off-line automatic kinematic chain calibration resorting to self-touch events, which was proven to be highly effective to optimize the robot's model Denavit-Hartenberg parameters. One setback of [16] is that it does not consider the joint angle measurements inaccuracies; apart from the requirement of a robot covered with a sensitive skin.

On-line solutions using on-board cameras have been studied [17], [18], [19], in which markers are used to easily detect the end-effector position; the inclusion of additional parts into the kinematic chain (*i.e.*, tools) has been considered as well [20]. Methods to perform on-line calibration, *e.g.*, during reaching tasks, based on contact information have also been studied. That is the case in [21] where they set to improve the robot's estimate of its configurations using an implicit *Manifold Particle Filter* informed by contact sensors during periods of persistent contact. In addition, goal-directed strategies in which the robot learns about its internal model during the execution of a goal-driven task, such as the ones presented in [22] (goal-directed exploration) and [23] (goal babbling), have been observed to enhance the body schema learning, for example, by reducing the time necessary for robot calibration convergence.

Vicente *et al.* [24] compare data from the robot's vision, and proprioception with a realistic 3D computer graphics model of the robot [25] in order to estimate simultaneously the robot's hand pose and kinematic model, making use of GPU programming to implement a *Particle Filter*. Kolev *et al.* [26] combine data acquired from proprioception, motion capture position and orientation, and force sensors, while interacting with objects in its vicinity, so as to build an internal simulation of the robot's configurations exploiting MuJoCo and estimating the model parameters values that better explain the visualized results.

We propose a novel approach to adapt the robot's body schema using proprioception and haptic sensors, capable of being executed online during robot's normal operations.

Information about contacts on known planar surfaces feed a low computational cost estimation method (Extended Kalman Filter) enabling real-time body schema adaptation.

III. PROBLEM STATEMENT

A. Body Schema Modeling

The adaptation of the body schema can be seen as an internal process that occurs in the mind of the robot using its own perception to achieve a better internal model representation of the self. We focus on the calibration of the arms and hands by exploiting haptic perception on the fingertips. The body schema, from a robotics perspective, is embedded as the kinematic chain from the root reference frame to the end-effector and it is used to derive the forward model (to predict from the motor commands where the end-effector is in the 3D task-space): $\mathbf{T}^e = \mathcal{K}(\boldsymbol{\theta})$; and the inverse model (to anticipate the motor commands to reach a given target in the 3D task-space): $\boldsymbol{\theta} = \mathcal{K}^{-1}(\mathbf{T}^e)$. Let us define \mathbf{T}^e as a 4x4 roto-translation matrix which encapsulates the pose of the end-effector on the root reference frame. Due to modulation errors we only get an estimation of the robot kinematics function ($\widehat{\mathcal{K}}(\cdot)$) based on the joint angles ($\boldsymbol{\theta}$) retrieved:

$$\mathbf{T}^e = \widehat{\mathcal{K}}(\boldsymbol{\theta}), \quad (1)$$

where $\mathcal{K}(\boldsymbol{\theta})$ is the true robot kinematics. However, due to the existence of calibration errors (bias), the real joints angles are different from the ones read from proprioception (joints encoders): $\boldsymbol{\theta} = \boldsymbol{\theta}^p + \boldsymbol{\beta}$, where $\boldsymbol{\theta}$ are the real angles values, $\boldsymbol{\theta}^p$ are the encoders readings (proprioception) and $\boldsymbol{\beta}$ are the angular offsets. To better estimate the robot kinematics we reformulate Eq. (1) to account for the offsets estimate $\widehat{\boldsymbol{\beta}}$:

$$\mathbf{T}^e = \widehat{\mathcal{K}}(\boldsymbol{\theta}^p + \widehat{\boldsymbol{\beta}}). \quad (2)$$

The parameter vector and our state (to be estimated recursively) is defined as follows:

$$\boldsymbol{\beta} = [\beta^1 \beta^2 \dots \beta^N]^T, \quad (3)$$

where N is the number of degrees of freedom of the robot's manipulator. Assuming the joint offsets to be slowly varying in time, we define the state-transition model as:

$$\boldsymbol{\beta}_t = \boldsymbol{\beta}_{t-1} + \boldsymbol{\varepsilon}_t, \quad (4)$$

where $\boldsymbol{\varepsilon}_t$ is a multivariate zero-mean Gaussian noise.

B. Observation Model

The observation model relates the system state $\boldsymbol{\beta}$ with a single measurement (z_k) from the tactile sensors. We assume that there is a planar surface described by:

$$\mathbf{x} \cdot \mathbf{n} - d = 0, \quad (5)$$

where $\mathbf{n} = [n_x, n_y, n_z]^T$ define the plane's normal vector ($\|\mathbf{n}\| = 1$), and d is the plane's minimum distance to the robot root frame. In a simulation environment, both \mathbf{n} and d are known *a priori*. On real robot experiments, vision sensing can be used to estimate the surface's pose on the robot vicinity, *e.g.*, using the Aruco marker [27] or computing a planar fit on depth point clouds from stereo vision.

When a contact occurs, we are ensuring that the arm's end-effector 3D position (\mathbf{x}^e) respects Eq. (5). However, due to errors in the kinematic model, each set of coordinates $\widehat{\mathbf{x}}_k^e$ at an instant k , follows the equation:

$$\widehat{\mathbf{x}}_k^e \cdot \mathbf{n} - d = \alpha_k, \quad (6)$$

where α_k is the error produced by the model inaccuracies.

The observation model is then defined as:

$$z_k(\boldsymbol{\theta}_k^p + \widehat{\boldsymbol{\beta}}_t) = \alpha_k + \delta_k \quad (7)$$

where $\widehat{\mathbf{x}}_k^e$ is retrieved using the forward kinematics (Eq. (2)), $\widehat{\boldsymbol{\beta}}_t$ are the offsets estimation at time instate t and δ_k is random Gaussian noise associated to an observation.

IV. APPROACH

We estimate the angular offsets $\boldsymbol{\beta}$ by exploiting contact constraints obtained at each end-effector contact with a surface. The strategy devised can be divided into two steps: i) a goal babbling exploration towards the target planar surface, stopping when *tactile stimuli* in the index finger occurs; and ii) a learning phase where an Extended Kalman Filter is fed with multisensory input (*i.e.*, proprioception, surface characteristics and haptic feedback) adapting the state $\boldsymbol{\beta}$.

A. Workspace Exploration

The robot performs a goal babbling movement towards the desired surface using the joint space ($\boldsymbol{\theta}$) as the input command. The generation of the babbling movement is based on the geometric Jacobian ($\mathbf{J}_e(\boldsymbol{\theta})$) of the manipulator:

$$\dot{\mathbf{x}}^e = \mathbf{J}_e(\boldsymbol{\theta}) \cdot \dot{\boldsymbol{\theta}} \quad ; \quad \mathbf{J}_e(\boldsymbol{\theta}) = \begin{bmatrix} \mathbf{J}_e^v(\boldsymbol{\theta})_{3 \times N} \\ \mathbf{J}_e^\omega(\boldsymbol{\theta})_{3 \times N} \end{bmatrix}_{6 \times N}, \quad (8)$$

which relates the N joint velocities ($\dot{\boldsymbol{\theta}}$) with the end-effector task-space velocities ($\dot{\mathbf{x}}^e$). The sub-matrices $\mathbf{J}_e^v(\boldsymbol{\theta})$ and $\mathbf{J}_e^\omega(\boldsymbol{\theta})$ describe the linear and angular task-space velocities for a given $\dot{\boldsymbol{\theta}}$, respectively. To ensure that the babbling movement is in the direction of the target surface we test the condition:

$$(\mathbf{J}_e^v(\boldsymbol{\theta}) \cdot \dot{\boldsymbol{\theta}})^T \cdot \mathbf{n} \leq 0, \quad (9)$$

where \mathbf{n} is the surface normal. If the condition is not satisfied, the motor command is discarded. The exploration stops when a contact is detected by the haptic sensors.

B. Parameter Estimation - Extended Kalman Filter (EKF)

The estimation of the offsets in Eq (3) can be performed with an EKF, commonly used for online parameter estimation (as seen in [28]), assuming that each β^i is distributed through multivariate normal distributions (with mean μ and covariance $\boldsymbol{\Sigma}$). Using the dynamics in Eq. (4) and observation model (Eq. (7)), we get the following EKF equations:

1) Prediction:

$$\overline{\boldsymbol{\beta}}_t = \widehat{\boldsymbol{\beta}}_{t-1} + \boldsymbol{\varepsilon}_t, \quad (10a)$$

$$\overline{\boldsymbol{\Sigma}}_t = \boldsymbol{\Sigma}_{t-1} + \mathbf{Q}_t, \quad (10b)$$

2) Kalman Gain and Update:

$$\mathbf{K}_t = \overline{\boldsymbol{\Sigma}}_t \mathbf{H}_t^T (\mathbf{H}_t \overline{\boldsymbol{\Sigma}}_t \mathbf{H}_t^T + \mathbf{R}_t)^{-1}, \quad (10c)$$

$$\widehat{\boldsymbol{\beta}}_t = \overline{\boldsymbol{\beta}}_t + \mathbf{K}_t (\mathbf{0} - \mathbf{z}_t), \quad (10d)$$

$$\boldsymbol{\Sigma}_t = (\mathbf{I} - \mathbf{K}_t \mathbf{H}_t) \overline{\boldsymbol{\Sigma}}_t, \quad (10e)$$

where $\widehat{\boldsymbol{\beta}}_t$ and $\boldsymbol{\Sigma}_t$ are the current offsets estimation and covariance matrix, respectively. \mathbf{Q}_t and \mathbf{R}_t are positive semi-definite covariance matrices and \mathbf{z}_t and \mathbf{H}_t encapsulate a set of observations. When a contact is detected and the joint encoders readings are retrieved, we acquire an observation (z_k) as well as $\mathbf{H}_k = \nabla z_k(\boldsymbol{\theta}_k^p + \widehat{\boldsymbol{\beta}}_t)$. We can rewrite \mathbf{H}_k as:

$$\mathbf{H}_k = \mathbf{n} \cdot \mathbf{J}_e^v(\boldsymbol{\theta}_k^p + \widehat{\boldsymbol{\beta}}_t), \quad (11)$$

where $\mathbf{J}_e^v(\boldsymbol{\theta}_k^p + \widehat{\boldsymbol{\beta}}_t)$ is the sub-matrix defined in Eq. (8).

We evaluate 3 strategies for new data incorporation:

1) *Aggregation of Multiple Observations*: Coupling together a varying number of contact constraints (k) before a filter update step (t). The number of observations coupled in this manner influence matrices \mathbf{H}_t and \mathbf{z}_t dimensions:

$$\mathbf{H}_t = [\mathbf{H}_{k-n} \quad \cdots \quad \mathbf{H}_{k-1} \quad \mathbf{H}_k]^T, \quad (12a)$$

$$\mathbf{z}_t = [z_{k-n} \quad \cdots \quad z_{k-1} \quad z_k]^T, \quad (12b)$$

where t is the instant when we perform an estimation step. The number of contact detected up until t is $n+1$. Using only one observation ($n=0$) we have $\mathbf{H}_t \equiv \mathbf{H}_k$ and $\mathbf{z}_t \equiv z_k$.

2) *Estimation Differential Entropy Evaluation*: Upon each contact, we get \mathbf{z}_t and \mathbf{H}_t and compute the predicted next step estimation covariance matrix $\boldsymbol{\Sigma}_t$. Following the approach used in [29], we decide to incorporate the new data if the current estimation differential entropy decreases when compared with the previous estimation:

$$\frac{1}{2} \log_e \frac{|\boldsymbol{\Sigma}_{t-1}|}{|\boldsymbol{\Sigma}_t|} > 0, \quad (13)$$

and discard new data that does not bring innovative information. Here $|\cdot|$ denotes a matrix determinant and $\boldsymbol{\Sigma}_{t-1}$ is the current estimation covariance matrix.

3) *Anti-Windup Control (A-W)*: A common problem in recursive parameter estimation is windup in the system state covariance matrix $\boldsymbol{\Sigma}_t$ during periods of poor excitation. This phenomenon happens when some eigenvalues of $\boldsymbol{\Sigma}_t$ increase uncontrollably to large values when highly correlated data is incorporated, making the filter oversensitive to noise and with long transients when relevant data is obtained, leading the system to incorrect estimates. In [30] a technique is described in order to avoid windup associated to recursive estimation methods, such as the Recursive Least Squares (which can be recast into a EKF). They propose controlling the parameter random walk covariance matrix, $\mathbf{Q}(t)$, so as to get $\boldsymbol{\Sigma}_t$ to achieve a constant pre-defined covariance matrix, \mathbf{P}_d , thus avoiding it to get unacceptable large eigenvalues. We use the same technique adapted to the EKF framework:

$$\mathbf{Q}(t) = \frac{\mathbf{P}_d \mathbf{H}_t \mathbf{H}_t^T \mathbf{P}_d}{\mathbf{R}(t) + \mathbf{H}_t^T \mathbf{P}_d \mathbf{H}_t}. \quad (14)$$

TABLE I

FINAL ESTIMATION MEAN (μ) AND STANDARD DEVIATION (σ) VALUES.

| Estimation method | One Surface | | Three Surfaces | |
|---|---------------|------------------|----------------|------------------|
| | $\mu[^\circ]$ | $\sigma[^\circ]$ | $\mu[^\circ]$ | $\sigma[^\circ]$ |
| 7C (a.) | 5.05 | 1.76 | 3.36 | 1.41 |
| SC (b.) | 4.85 | 2.42 | 2.30 | 1.00 |
| SC-E (c.) | 5.08 | 1.34 | 5.00 | 2.06 |
| VC-E (d.) | 3.53 | 2.28 | 2.41 | 1.02 |
| SC-AW (e.) | 4.63 | 1.70 | 2.67 | 0.80 |
| SC-EAW (f.) | 4.11 | 1.66 | 2.20 | 0.74 |
| Without calibration ($\hat{\beta} = \mathbf{0}_{7 \times 1}$) | 11.74 | - | 11.74 | - |

V. EXPERIMENTAL SETUP

The algorithms developed are tested in an iCub simulator [31] which is provided with proprioception, visual and tactile sensors. To communicate with the simulator we use the YARP middleware [32]. The simulation setup is composed of three reachable surfaces with *a priori* known parameters (\mathbf{n} and d), relative to the robot's root frame, which provide a rich environment for the robot to acquire contact constraints: $\mathbf{n}^1 = (\frac{\sqrt{2}}{2}, 0, \frac{\sqrt{2}}{2})$ and $d^1 = \frac{-\sqrt{2}}{8}\text{m}$, $\mathbf{n}^2 = (\frac{\sqrt{2}}{2}, \frac{\sqrt{2}}{2}, 0)$ and $d^2 = \frac{-3\sqrt{2}}{10}\text{m}$, $\mathbf{n}^3 = (0, -1, 0)$ and $d^3 = -0.05\text{m}$. For the first set of experiments, we make the robot constantly reach for the surface described by \mathbf{n}^1 and d^1 . We then perform a second set of experiments where the contact events alternate between all three surfaces. Figure 1 shows the simulated iCub robot reaching for these surfaces.

We control the robot's left arm and define its left index fingertip to be the manipulator's end effector. The angular offsets on the seven DoF of the iCub's left arm are artificially simulated and the index finger joints are fixed. We define $\beta = [-11, 11, -7, -17, -7, -17, 7]^T$ deg, whose values have the same order of magnitude of the calibration errors we typically encounter on the real robot. All simulations are performed relative to these offsets, except for the last set of experiments, where we use 2 different artificially introduced offsets sets in order to test the strategy robustness.

We present next the simulated results for the devised calibration strategy, comparing all new data incorporation methods proposed (see subsection V-A), running a total of ten simulations for each method. For each experiment, we perform a total of 45 contacts (49 for the 7-contact setting). After each filter update, we compute the global estimation root mean squared error (RMSE) relative to the real offsets:

$$\text{RMSE} = \sqrt{\frac{1}{7} \sum_{i=1}^7 (\hat{\beta}^i - \beta^i)^2}. \quad (15)$$

A. New Data Incorporation Methods

Next, we provide a detailed description of the different new data incorporations methods which are evaluated in the results section. These methods are the combination of one, two or three different strategies mentioned in IV-B:

a) 7-Contact (7C): Upon each contact detection, z_k and \mathbf{H}_k are stored in \mathbf{z}_t and \mathbf{H}_t , respectively. The system performs an estimation step after it collects 7 contact constraints (equal to the number of the iCub's arm DoFs).

b) Single Contact (SC): Upon each contact event, z_k and \mathbf{H}_k are fed to the filter and an update step is performed.

c) Single Contact with Entropy (SC-E): Similar to the previous technique, but now for each new data obtained the system computes the predicted next step estimation covariance matrix and evaluates whether or not the new observation actively contributes to the estimation differential entropy reduction using Eq. (13). If the condition is not satisfied, the new observation is discarded.

d) Varying-Contact with Entropy (VC-E): Equivalent to the previous method, but each time a new observation fails to reduce the global estimation differential entropy, instead of being discarded, z_k and \mathbf{H}_k are added to the matrices \mathbf{z}_t and \mathbf{H}_t , respectively. Every time new data is obtained, the system evaluates if \mathbf{z}_t and \mathbf{H}_t are able to reduce the entropy of the next step estimation. If so, an update step is performed regarding all previously stored observations.

e) Single Contact with A-W (SC-AW): Equivalent to the Single Contact Estimation method, but \mathbf{Q}_t is controlled with the anti-windup technique described in Eq. (14), rather than being a predefined matrix.

f) Single Contact with Entropy and A-W (SC-EAW): The system discards every new observation data which fails to reduce the next step estimation differential entropy, and controls \mathbf{Q}_t matrix so as to avoid estimation windup from uncorrelated measures.

VI. RESULTS

We evaluate the results of β estimation for contacts in a single, and in three different surfaces¹. All experimental results are shown in Table I, which depicts each new data incorporation strategy global performance, providing the β estimation error mean (μ) and standard deviation (σ) over 10 experiments after 45 contact events.

A. Contacts over a single surface

We start by evaluating the results of β estimation with the method 7C. In Fig. 2(a), the mean estimation error μ (in blue), and the standard deviation σ (in shaded-red) over the 10 experiments with 49 contact events each (*i.e.*, 7 filter update steps) can be seen. The estimation error decreases slowly over each estimation step, and the model inaccuracies are reduced by 50% (RMSE \approx 5.87 deg) after 35 contacts.

The results for method SC can be seen in Fig. 2(b), which show a worse performance. The system keeps a slow steady error descend during the whole estimation, reducing the estimation absolute error by 50% after 37 contacts. Moreover, σ remains relatively high for all t , due to the slow reaction of the filter against estimation steps taken in the wrong direction during periods of poor excitation.

We try to improve method SC by evaluating the estimation differential entropy (Fig. 2(c)) or using the A-W control

¹a video can be found in <https://youtu.be/EFx00mRKTQg>

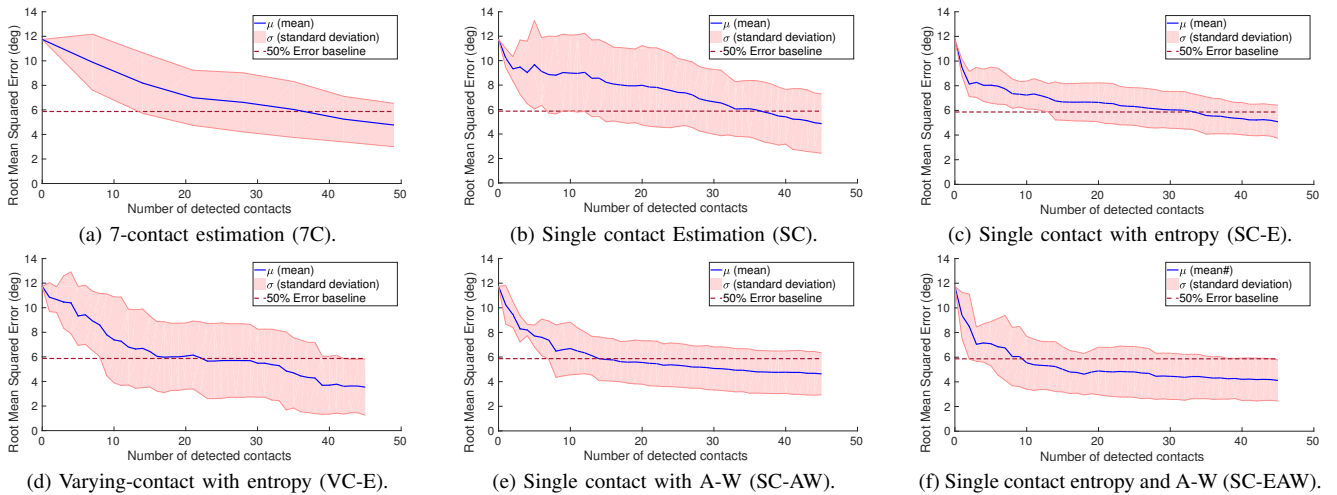


Fig. 2. RMSE (mean and standard deviation) over 10 experiment for each data incorporation method (V-A) for β estimation from contacts on one surface.

technique (Eq. (14)) (Fig. 2(e)). For the first solution (method **SC-E**), we conclude that it is able to stabilize the filter performance, since the global estimation σ is reduced compared to the simple single contact setting (see Table I). However, this happens at the cost of the filter converging sooner to a minimum, since it is not able to easily find observations which reduce the estimation entropy. Furthermore, the estimation error does not increase at any moment, opposed to the simpler method **SC**. The later solution (method **SC-AW**) achieves a better performance as well, being able to stabilize the filter. Its key improvements are: i) higher pronounced error reduction slope up until the 8th contact; ii) its able to reduce the absolute error by 50% after 14 contacts, also improving the final solution after 45 contacts (see Table I).

The method **VC-E** is a mixed model combining the entropy evaluation with the method **7C**. We enable the filter to adapt, coupling together a sufficient number of observations to perform an estimation update step with lower entropy. The estimation keeps a steady error descend up until the 16th contact (reducing the model inaccuracies by 50%), slowing the pace for the next contacts (see Fig. 2(d)).

Finally, in Fig. 2(f), we see the results of combining both the A-W control technique and estimation entropy evaluation on a single contact strategy (method **SC-EAW**). We are able to notice three key features: i) the system is able to converge to a lower overall estimation minimum (reducing the estimation error by 15% compared to the single contact setting, and 65% overall, after 45 contact events), ii) the overall experiments σ is 30% lower compared to method **SC**, and iii) the system converges faster to a minimum (requires 10 steps to reduce the model inaccuracies by 50%). Combining both techniques we are able to get a more stable and precise filter. Fig. 3(a) helps us to visually compare the performance of all methods.

B. Contacts over three different surfaces

By broadening the robot spatial exploration in order to perform contacts on 3 surfaces, we expect an overall better β estimation performance, since contact constraints obtained in

this manner provide to the filter richer information. Looking at Fig. 3(b), we are able to visually analyze the different methods performance in this scenario. We can clearly assess from Fig. 3(b) that the methods **7C** and **SC-E** are the ones which benefit less from information acquired from contacts on 3 different surfaces since they both converge to the highest estimation errors minima. The **7C** setting has a steady slow error reduction slope due to not being able to quickly compensate for estimation steps given on wrong directions. The **SC-E** estimation converges early (5th contact) to a local minimum, not being able to easily find relevant observations from there. The best results are obtained for the single contact setting with both estimation entropy evaluation and anti-windup control techniques, reducing both the estimation error by 45% relative to the single surface scenario (and 80% overall), and presenting the lowest overall σ value.

Finally, in Fig. 3(c) we see the results of using the method **SC-EAW** for β estimation of 3 different artificially introduced offsets readings (10 experiments for each set). Up until the 60th contact event, all experiments reach an estimation minimum; moreover, independently of the true readings offsets, the filter is always able to reduce the estimation error to approximately 2.5deg, illustrating the reliability of the devised strategy.

VII. CONCLUSIONS AND FUTURE WORK

We devise a novel approach for online body schema adaptation, implemented on the iCub humanoid robot, leading to subsequent improvements in the end-effector pose estimation. The robot's arm offsets estimation is performed using an EKF fed with contact constraints obtained during the execution of reaching tasks. We rely on typical humanoid robot's embedded sensors (tactile and proprioception). Our strategy is inspired by the human incremental learning process of their own body schema, as we use tactile feedback in order to enable the robot to learn about its internal model.

One can conclude from our experiments that by making the robot perform a spatial exploration on an information richer workspace (*i.e.*, with various surfaces) it is more

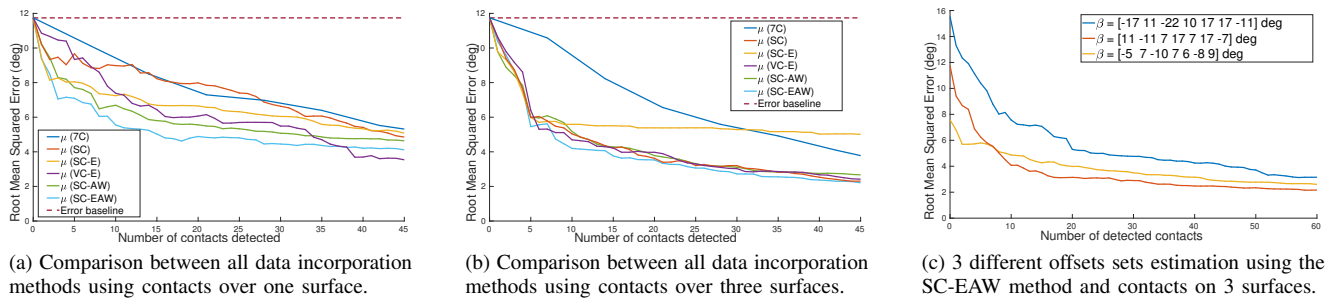


Fig. 3. β estimation performances comparison between all data incorporation methods and for contacts contacts events over one or three surfaces.

effective in reducing its model inaccuracies. Overall, our simulation experiments show that we can reduce the model inaccuracies up to 80% by performing contacts on 3 different surfaces, and up to 63% for contacts on a single surface.

In future work we intend to test the developed strategy on the real-world scenario, making use of vision sensing to extract information about surfaces' poses. Another possible direction would be to implement a different adaptive estimation filter from the EKF, like the Unscented Kalman Filter or the Particle Filter, to cope with deviations from Gaussianity of the estimated parameters distribution.

ACKNOWLEDGMENTS

This work was partially supported by FCT (UID/EEA/50009/2013 and PD/BD/135115/2017), and by EPSRC UK (project NCNR, National Centre for Nuclear Robotics, EP/R02572X/1). We acknowledge the support of NVIDIA with the donation of a GPU.

REFERENCES

- [1] G. Berlucchi and S. Aglioti, "The body in the brain: neural bases of corporeal awareness," *TINS*, no. 20(12), pp. 560–564, 1997.
- [2] P. J. Marshall and A. N. Meltzoff, "Body maps in the infant brain," *Trends Cogn. Sci.*, no. 19(9), pp. 499–505, 2015.
- [3] R. Joseph, "Fetal brain behavior and cognitive development," *Developmental Review*, vol. 20, pp. 81–98, 2000.
- [4] C. von Hofsten, "An action perspective on motor development," *Trends Cogn. Sci.*, vol. 8, pp. 266–272, 2004.
- [5] A. De Luca and F. Flacco, "Integrated control for phri: Collision avoidance, detection, reaction and collaboration," in *IEEE/RAS-EMBS BioRob*, 2012, pp. 288–295.
- [6] G. Metta, L. Natale, F. Nori, G. Sandini, D. Vernon, L. Fadiga, C. von Hofsten, K. Rosander, M. Lopes, J. Santos-Victor, A. Bernardino, and L. Montesano, "The icub humanoid robot: an open-systems platform for research in cognitive development," *Neural Netw.*, vol. 23, 2010.
- [7] A. Miller and B. Leibowitz, "Integration of vision, force and tactile sensing for grasping," *Int. J. Intell. Mach.*, vol. 4, pp. 129–149, 1999.
- [8] F. Reinhart and J. Steil, "Reaching movement generation with a recurrent neural network based on learning inverse kinematics for the humanoid robot icub," in *Int. Conf. on Humanoid Robots*. IEEE, 2013, pp. 323–330.
- [9] T. Schmidt, A. Newcombe, and D. Fox, "Dart: Dense articulated real-time tracking," in *RSS*, 2014.
- [10] M. Peniak and A. Cangelosi, "Scaling-up action learning neuro-controllers with gpus," in *IJCNN*. IEEE, 2014, pp. 2519–2524.
- [11] T. Schmidt, K. Hertkorn, R. Newcombe, Z. Marton, M. Suppa, and D. Fox, "Depth-based tracking with physical constraints for robot manipulation," in *2015 IEEE ICRA*, pp. 119–126.
- [12] M. Hoffmann, H. Marques, A. Arieta, H. Sumioka, M. Lungarella, and R. Pfeifer, "Body schema in robotics: a review," *IEEE TAMD*, vol. 2, no. 4, pp. 304–324, 2010.
- [13] P. Lanillos, E. Dean-Leon, and G. Cheng, "Enactive self: a study of engineering perspectives to obtain the sensorimotor self through enaction," in *IEEE ICDL-Epirob*, 2017.
- [14] Y. Meng and H. Zhuang, "Autonomous robot calibration using vision technology," *Robot Comput. Integr. Manuf.*, vol. 23, no. 4, pp. 436–446, 2007.
- [15] Y. Bai, H. Zhuang, and S. Roth, "Experiment study of puma robot calibration using a laser tracking system," in *2003 IEEE SMCia*, 2003, pp. 139–144.
- [16] A. Roncone, M. Hoffmann, U. Pattacini, and G. Metta, "Automatic kinematic chain calibration using artificial skin: self-touch in the icub humanoid robot," in *2014 IEEE ICRA*, pp. 2305–2312.
- [17] S. Ulbrich, V. de Angulo, T. Asfour, and C. Torras, "Rapid learning of humanoid body schemas with kinematic bezier maps," in *IEEE-RAS Intl. Conf. on Humanoid Robots*, 2009, pp. 431–438.
- [18] L. Jamone, L. Natale, G. Metta, F. Nori, and G. Sandini, "Autonomous online learning of reaching behavior in a humanoid robot," *Intl. J. of Humanoid Robotics*, no. 9(3), pp. 125017(1–26), 2012.
- [19] L. Jamone, M. Brandao, L. Natale, K. Hashimoto, G. Sandini, and A. Takanishi, "Autonomous online generation of a motor representation of the workspace for intelligent whole-body reaching," *Rob. Auton. Syst.*, no. 64(4), pp. 556–567, 2014.
- [20] L. Jamone, B. Damas, N. Endo, V. Santos, and A. Takanishi, "Incremental development of multiple tool models for robotic reaching through autonomous exploration," *Paladyn*, no. 3, pp. 113–127, 2013.
- [21] M. Klingensmith, C. Koval, S. Srinivasa, S. Pollard, and M. Kaess, "The manifold particle filter for state estimation on high-dimensional implicit manifolds," *2017 IEEE ICRA*, pp. 4673–4680.
- [22] L. Jamone, L. Natale, K. Hashimoto, G. Sandini, and A. Takanishi, "Learning task space control through goal directed exploration," in *2011 IEEE ROBOT*, pp. 702–708.
- [23] M. Rolf, "Goal babbling with unknown ranges: A direction-sampling approach," in *2013 IEEE ICDL*, pp. 1–7.
- [24] P. Vicente, L. Jamone, and A. Bernardino, "Online body schema adaptation based on internal mental simulation and multisensory feedback," *Front. robot. AI*, vol. 3, p. 7, 2016.
- [25] —, "Robotic hand pose estimation based on stereo vision and gpu-enabled internal graphical simulation," *J. Intell. Robotic Syst.*, vol. 83, no. 3-4, pp. 339–358, 2016.
- [26] S. Kolev and E. Todorov, "Physically consistent state estimation and system identification for contacts," in *2015 IEEE-RAS Intl. Conf. on Humanoid Robots*, pp. 1036–1043.
- [27] S. Jurado, R. Salinas, J. Cuevas, and J. Jiménez, "Automatic generation and detection of highly reliable fiducial markers under occlusion," *Pattern Recognition*, vol. 47, no. 6, pp. 2280–2292, 2014.
- [28] L. Ljung, "Asymptotic behavior of the extended kalman filter as a parameter estimator for linear systems," *IEEE Trans. Automat. Contr.*, vol. 24, no. 1, pp. 36–50, 1979.
- [29] J. Maye, H. Sommer, G. Agamnonni, R. Siegwart, and P. Furgale, "Online self-calibration for robotic systems," *Int. J. Robotics Res.*, vol. 35, no. 4, pp. 357–380, 2016.
- [30] B. Stenlund and F. Gustafsson, "Avoiding windup in recursive parameter estimation," *Preprints of reglermöte 2002*, pp. 148–153, 2002.
- [31] V. Tikhonoff, A. Cangelosi, P. Fitzpatrick, G. Metta, L. Natale, and F. Nori, "An open-source simulator for cognitive robotics research: the prototype of the icub humanoid robot simulator," in *Proceedings of the 8th workshop on PerMIS*. ACM, 2008, pp. 57–61.
- [32] G. Metta, P. Fitzpatrick, and L. Natale, "Yarp: yet another robot platform," *IJARS*, vol. 3, no. 1, p. 8, 2006.